

Photovoltaic Devices Using Semiconducting Polymers Containing Head-to-Tail-Structured Bithiophene, Pyrene, and Benzothiadiazole Derivatives

Ji-Hoon Kim,¹ Sunyoung Lee,² In-Nam Kang,³ Moo-Jin Park,⁴ Do-Hoon Hwang¹

¹Department of Chemistry and Chemistry Institute for Functional Materials, Pusan National University, Busan 609-735, Republic of Korea

²Department of Applied Chemistry, Kumoh National Institute of Technology, Kumi 730-701, Korea

³Department of Chemistry, The Catholic University of Korea, Bucheon 420-743, Korea

⁴Polymer Science and Engineering Program, KAIST, Daejeon 305-701, Korea

Correspondence to: D.-H. Hwang (E-mail: dohoonhwang@pusan.ac.kr)

Received 5 February 2012; accepted 14 April 2012; published online

DOI: 10.1002/pola.26130

ABSTRACT: An alternating copolymer composed of head-to-tail-structured 3,4'-dihexyl-2,2'-bithiophene (DHBT) and pyrene units [poly(DHBT-*alt*-PYR)] was synthesized using a Stille coupling reaction for use in photovoltaic devices as a p-type donor. For the reduction of the bandgap energy of poly(DHBT-*alt*-PYR), 4,7-bis(3'-hexyl-2,2'-bithiophen-5-yl)benzo[*c*][1,2,5]thiadiazole (BHBTBT) units were introduced into the polymer. Poly(DHBT-*co*-PYR-*co*-BHBTBT)s were synthesized using the same polymerization reaction. The synthesized polymers were soluble in common organic solvents and formed smooth thin films after spin casting. The optical bandgap energies of the polymers were obtained from the onset absorption wavelengths. The measured optical bandgap energy of poly(DHBT-*alt*-PYR) was 2.47 eV. As the BHBTBT content in the *ter*-polymers increased, the optical bandgap energies of the resulting polymers decreased. The bandgap energies of poly(50DHBT-

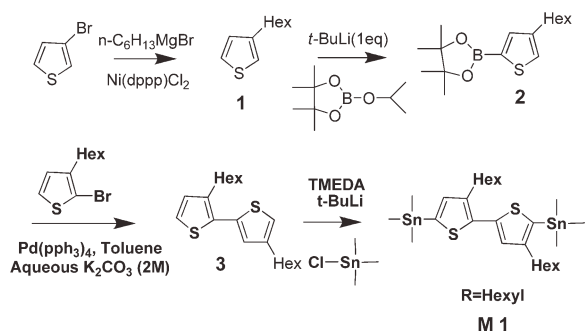
co-40PYR-*co*-10BHBTBT) and poly(50DHBT-*co*-20PYR-*co*-30BHBTBT) were 1.84 and 1.73 eV, respectively. Photovoltaic devices were fabricated with a typical sandwich structure of ITO/PEDOT:PSS/active layer/LiF/Al using the polymers as electron donors and [6,6]-phenyl C₇₁-butyric acid methyl ester as the electron acceptor. The device using poly(50DHBT-*co*-20PYR-*co*-30BHBTBT) showed the best performance among the fabricated devices, with an open-circuit voltage, short-circuit current, fill factor, and maximum power conversion efficiency of 0.68 V, 5.54 mA/cm², 0.35, and 1.31%, respectively. © 2012 Wiley Periodicals, Inc. *J Polym Sci Part A: Polym Chem* 000: 000–000, 2012

KEYWORDS: bulk heterojunction; conjugated polymers; copolymerization; electrochemistry; organic solar cell; organic thin-film transistor; polyaromatics; synthesis

INTRODUCTION Organic semiconductors have attracted extensive scientific interest for applications in organic electronics and optoelectronics, including for organic thin-film transistors (OTFTs) and organic photovoltaic cells (OPVs).^{1–13} In particular, polymer semiconductors have been studied because of advantages such as their chemical tenability, compatibility with plastic substrates, structural flexibility, mechanical stability, and cost-effective manufacture by using various printing technologies such as roll-to-roll process.^{14,15} Increase of the power conversion efficiency (PCE) and stability of OPVs are currently important key issues for their practical application.¹⁶

Although the conventional blends of poly(3-hexylthiophene) and [6,6]-phenyl-C₆₁-butyric acid methyl ester have reached PCEs of up to 5%,^{17–19} further increase in the PCE is rather difficult because of their limited photocurrent generation and intrinsic absorption properties. Therefore, an alternative

approach for improving the performance is to use low-bandgap donor-acceptor polymeric materials; higher efficiencies up to 7.7% have been obtained with such polymers.²⁰ The short-circuit current density (J_{sc}), open-circuit voltage (V_{oc}), and fill factor (FF) are the key parameters for OPV devices, because the PCE of the device is proportional to the values of these three parameters. Broadening the response wavelength range of an OPV device by using conjugated side chains^{21,22} or narrow-bandgap conjugated polymers^{23,24} is an effective way to realize high J_{sc} values. Conjugated polymers with low highest occupied molecular orbital (HOMO) levels are helpful in realizing high V_{oc} and PCE values, as the V_{oc} value of an OPV is directly proportional to the offset between the HOMO level of the electron donor and the LUMO level of the electron acceptor.²⁵ Poly[2,7-silafluorene-*alt*-4,7-di(2'-thienyl)-2,1,3-benzothiadiazole],²⁶ poly[2,7-(9-(2'-ethylhexyl)-9-hexyl-fluorene)-*alt*-5,5-(4',7',-di-2-thienyl-2',1',3'-benzothiadiazole)],²⁷ and poly[[9-(1-octylonyl)-9H-



SCHEME 1 Synthetic routes and chemical structure of M1.

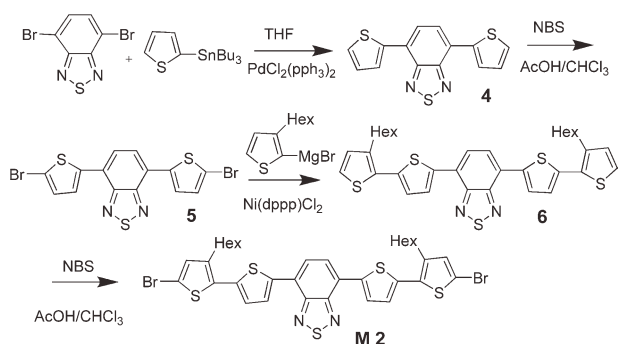
carbazole-2,7-diyl]-2,5-thiophenediyl-2,1,3-benzothiadiazole-4,7-diyl-2,5-thiophenediyl]²⁸ are three excellent examples of this concept. Consequently, by using conjugated polymers with lower HOMO levels and narrow bandgaps, high PCEs have been realized in different families of conjugated polymers.^{29,30}

Recently, many pyrene-containing molecules and polymers have been synthesized for diverse organic electronic devices such as organic light-emitting diodes and OTFTs, because of their unique electrical properties that are due to the delocalized π -conjugated system.^{31–33} Pyrene also has a flat structure and a relatively deep HOMO energy level, so we expected that the introduction of pyrene into conjugated polymers could lower the HOMO energy level, and that OPV devices using pyrene-containing polymers would show high open-circuit voltages. In this study, an alternating copolymer composed of head-to-tail-structured 3,4'-dihexyl-2,2'-bithiophene (DHBT) and pyrene units [poly(DHBT-*alt*-PYR)] was synthesized using a Stille coupling reaction. To reduce the bandgap energy of poly(DHBT-*alt*-PYR), we also introduced 4,7-bis(3'-hexyl-2,2'-bithiophen-5-yl)benzo[*c*][1,2,5]-thiadiazole (BHBTBT) units into the polymer. Poly(DHBT-*co*-PYR-*co*-BHBTBT)s were synthesized using the same polymerization reaction. The synthetic route and structures of the polymers are shown in Schemes 1–3.

EXPERIMENTAL

Materials

3-Bromothiophene, 1-bromohexane, *N*-bromosuccinimide (NBS), 1,3-bis(diphenylphosphino)propane nickel(II) chlo-



SCHEME 2 Synthetic routes and chemical structure of M2.

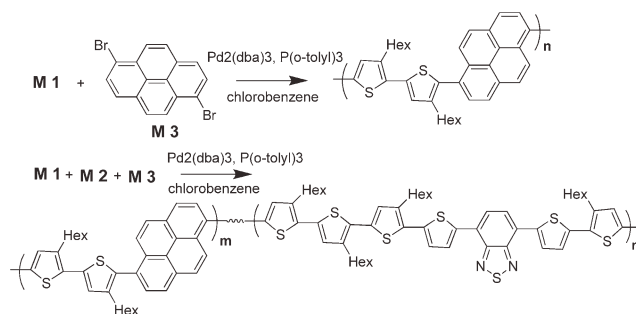
ride, pyrene, 2-(tributylstannyl)thiophene, bromine, trimethyltinchloride (1.0 M in tetrahydrofuran, THF), anhydrous chlorobenzene, *tert*-butyllithium (*t*-BuLi, 1.7 M in hexane), 2,1,3-benzothiadiazole, 2-isopropoxy-4,4,5,5-tetramethyl-1,3,2-dioxaborolane, and tetrakis(triphenylphosphine)palladium were purchased from Aldrich and were used without further purification. [6,6]-Phenyl C₇₁-butyric acid methyl ester (PC₇₁BM) was purchased from Nano-C.

Instrumentation

¹H and ¹³C NMR spectra were recorded on a Varian Mercury Plus 300 MHz spectrometer, and the chemical shifts were recorded in units of ppm with chloroform as the internal standard. The absorption spectra were measured using a JASCO JP/V-570 model. The molecular weights of the polymers were determined by gel permeation chromatography (GPC) analysis relative to a polystyrene standard using a Waters high-pressure GPC assembly (model M590). Thermal analyses were carried out on a Mettler Toledo TGA/SDTA 851° analyzer under a N₂ atmosphere with heating rates of 10 °C/min. Cyclic voltammetry (CV) was performed on a CH Instruments Electrochemical Analyzer. The CV measurements were carried out in acetonitrile solutions containing 0.1 M tetrabutylammonium tetrafluoroborate (TBABF₄) as the supporting electrolyte, using Ag/AgNO₃ as the reference electrode, a platinum wire as the counter electrode, and a platinum working electrode.

Fabrication of OTFT Devices

OTFTs were fabricated using a bottom-contact geometry device (channel length $L = 12 \mu\text{m}$ and width $W = 120 \mu\text{m}$). The source and drain contacts were gold (100 nm), and the dielectric was silicon oxide (SiO₂) with a thickness of 300 nm. The SiO₂ surface was cleaned, dried, and pretreated with a solution of 10.0 mM octyltrichlorosilane (OTS-8) in toluene at room temperature for 2 h under a N₂ atmosphere to produce nonpolar and smooth surfaces onto which the polymers could be spin coated. The polymers were dissolved in chloroform to a concentration of 0.5 wt %. Films of the organic semiconductors were spin coated at 1000 rpm for 50 s to a thickness of 60 nm. All the device fabrication procedures and measurements were carried out in air at room temperature.



SCHEME 3 Synthetic routes and chemical structures of the polymers.

Fabrication of Photovoltaic Devices

Composite solutions (1:3 weight ratio) of the polymers and PC₇₁BM were prepared using 1,2-dichlorobenzene as the solvent. The concentration was controlled adequately in the range of 1.0–2.0 wt %. The polymer photovoltaic devices were fabricated with a typical sandwich structure of indium tin oxide (ITO)/(3,4-ethylenedioxythiophene):poly(styrene-sulfonate) (PEDOT:PSS)/active layer/LiF/Al. The ITO-coated glass substrates were cleaned using a routine cleaning procedure, including sonication in detergent followed by distilled water, acetone, and 2-propanol. A 45-nm-thick layer of PEDOT:PSS (Baytron P) was spin coated on a cleaned ITO substrate after exposure of the ITO surface to ozone for 10 min. The PEDOT:PSS layer was baked on a hot plate at 140 °C for 10 min. The active layer was spin coated from the predissolved composite solution after filtering through 0.45- μ m PP syringe filters. The device structure was completed by deposition of 0.6 nm of LiF and a 120 nm of Al cathode as the top electrode onto the polymer active layer under a vacuum of 3×10^{-6} Torr in a thermal evaporator. The current density–voltage (*J*–*V*) characteristics of all the polymer photovoltaic cells were measured under the illumination of AM 1.5 G solar light (100 mW/cm²) by an Oriel 1000 W solar simulator. Electrical data were recorded using a Keithley 236 source-measure unit, and all characterizations were carried out in an ambient environment. The illumination intensity used was calibrated by a standard Si photodiode detector from PV Measurements, which was calibrated at NREL. The incident photon-to-current conversion efficiency (IPCE) was measured as a function of wavelength from 360 to 800 nm using an IPCE measurement system (PV Measurements) equipped with a halogen lamp as the light source; calibration was performed using a silicon reference photodiode. The thickness of the thin film was measured using a KLA Tencor Alpha-step IQ surface profilometer with an accuracy of ± 1 nm. The measurement was carried out after masking all but the active cell area of the fabricated device. All the characterization steps were carried out in an ambient laboratory atmosphere. The active area of the solar cells was 0.09 cm².

Synthesis of Monomers and Polymers

2-(4-Hexylthiophen-2-yl)-4,4,5,5-tetramethyl-1,3,2-dioxaborolane (**2**),³⁴ 4,7-di(thiophen-2-yl)benzo[*c*][1,2,5]thiadiazole (**4**),³⁵ and 4,7-di-2'-(5'-bromo)-thienyl-2,1,3-benzothiadiazole (**5**)³⁶ were synthesized according to the methods described in previous reports.

2-(4-Hexylthiophen-2-yl)-4,4,5,5-tetramethyl-1,3,2-dioxaborolane (**2**)

¹H NMR (300 MHz, CDCl₃, δ , ppm) 7.53 (s, 1H), 7.02 (s, 1H), 2.75 (t, 2H), 1.62 (m, 2H), 1.31 (s, 12H), 0.85 (t, 3H).

Synthesis of 3,4'-Dihexyl-2,2'-bithiophene (**3**)

Tetrakis(triphenylphosphine)palladium (0.097 g, 0.084 mmol) was inserted into a two-necked 100-mL round-bottomed flask in a dry box. A mixture of 2-(4-hexylthiophen-2-yl)-4,4,5,5-tetramethyl-1,3,2-dioxaborolane (1.0 g, 3.39 mmol), 2-bromo-3-hexylthiophene (1.26 g, 5.08 mmol), toluene (10 mL), and THF (20 mL) was added to the reactor. Aliquat 336 (0.113 g, 0.28

mmol) as the phase-transfer catalyst and 2 M aqueous sodium carbonate solution (8 mL) were also added to the reaction mixture, and the reaction solution was stirred at 80 °C for 24 h. Then, the reaction was quenched with methanol, the solvent was removed by rotary evaporation, and the residue was purified by reprecipitation several times in methanol, affording the product as a pale liquid (65%, yield).

¹H NMR (300 MHz, CDCl₃, δ , ppm) 7.62 (d, 1H), 7.60 (d, 1H), 7.09 (s, 1H), 6.98 (d, 1H), 2.78 (m, 2H), 2.42 (m, 2H), 1.53 (m, 4H), 1.21 (m, 12H), 0.88 (t, 6H).

Synthesis of 2,2'-Bis(trimethylstannyl)-3,3'-bis(hexyl)-5,5'-bithiophene (**M1**)

A 1.7 M solution of *t*-BuLi (10.99 mL, 18.68 mol) in *n*-hexane was added to a solution of 3,3'-dihexyl-2,5'-bithiophene (**1**) (2.5 g, 7.47 mmol) with *N,N,N',N'*-tetramethylethylenediamine (2.17 g, 18.68 mmol) in THF (60 mL) at –78 °C. The mixture was maintained at this temperature for 2 h, and then trimethyltin chloride (1.0 M) in THF (15.69 mL, 15.69 mmol) was added at –78 °C. The mixture was heated to room temperature and stirred for 12 h. The reaction was quenched with methanol, and the reaction solution was hydrolyzed and then extracted with diethylether and brine. The organic layer was separated, dried over anhydrous MgSO₄, and concentrated using a rotary evaporator. The yield of product obtained as a liquid was 58%.

¹H NMR (300 MHz, CDCl₃, δ , ppm) 7.43 (s, 1H), 6.95 (s, 1H), 2.73 (t, 2H), 2.55 (t, 2H), 1.60 (m, 4H), 1.26 (m, 12H), 0.85 (t, 6H), 0.35 (t, 18H). ¹³C NMR (CDCl₃, ppm) 137.8, 136.7, 136.4, 135.9, 131.4, 130.7, 126.1, 125.9, 35.1, 32.9, 30.1, 23.1, 22.5, 15.8, –8.17. Anal. calcd for C₂₆H₄₆S₂Sn₂: C, 47.3; H, 7.02; S, 9.71. Found: C, 46.9; H, 6.98; S, 9.69.

4,7-Di(thiophen-2-yl)benzo[*c*][1,2,5]thiadiazole (**4**)

¹H NMR (300 MHz, CDCl₃, δ , ppm): 7.84 (s, 2H), 7.43 (d, 2H), 7.21 (t, 2H), 6.61 (d, 2H).

4,7-Di-2'-(5'-bromo)-thienyl-2,1,3-benzothiadiazole (**5**)

¹H NMR (300 MHz, CDCl₃, δ , ppm) 7.80 (dd, 4H), 7.13 (d, 2H).

Synthesis of 4,7-Bis(5'-bromo-3'-hexyl-2,2'-bithiophen-5-yl)benzo[*c*][1,2,5]thiadiazole (**6** and **M2**)

A solution of 2-bromo-3-hexylthiophene (5.3 g, 21.44 mmol) in dry THF (30 mL) was added dropwise to magnesium (1.56 g, 64.32 mmol) in dry THF (10 mL) and the mixture was refluxed at 60 °C under nitrogen gas for 2 h. Then, this mixture was added slowly to a mixture of 4,7-bis(5-bromothiophen-2-yl)benzo[*c*][1,2,5]thiadiazole (**5**) (2.45 g, 5.36 mmol) and Ni(dppp)Cl₂ (0.23 g, 0.42 mmol) in dry THF (50 mL) at 0 °C. The mixture was refluxed at 60 °C for 12 h. The organic layer was extracted three times with diethyl ether. The combined organic layers were washed with brine and dried over anhydrous MgSO₄. The solvent was removed using a rotary evaporator, and the obtained product was purified by recrystallization from methanol to afford BHBTBT (**6**). The obtained BHBTBT (2.97 g, 4.69 mmol) (**6**) was dissolved in chloroform (60 mL) and acetic acid (5 mL) in a 250-mL one-necked flask with a magnetic stirrer. NBS

(1.84 g, 10.32 mmol) was added to the solution, which was then stirred for 2 h. The solvent was removed using the rotary evaporator, and the product was purified by flash silica gel column chromatography using a solvent (chloroform only) and obtained as a red powder by recrystallization from methanol. The product yield was 56%.

^1H NMR (300 MHz, CDCl_3 , δ , ppm): 8.09 (d, 2H), 7.86 (s, 2H), 7.16 (d, 2H), 6.93 (s, 2H), 2.78 (t, 4H), 1.65 (m, 4H), 1.39 (m, 4H), 1.31 (m, 8H), 0.90 (t, 6H). ^{13}C NMR (CDCl_3 , δ , ppm) 150.1, 145.8, 142.1, 140.8, 138.1, 137.9, 134.2, 132.1, 130.1, 129.5, 120.1, 33.5, 32.1, 31.0, 29.5, 28.4, 13.9. Anal. calcd for $\text{C}_{34}\text{H}_{34}\text{Br}_2\text{N}_2\text{S}_5$: C, 51.64; H, 4.33; Br, 20.21; N, 3.54; S, 20.27. Found: C, 51.60; H, 4.28; N, 3.21; S, 20.11.

Synthesis of 1,6-Dibromopyrene (M3)

Br_2 (4.94 g, 34.7 mmol) was added to a stirred solution of pyrene (5 g, 13.88 mmol) in carbon tetrachloride (200 mL) in darkness. The mixture was stirred at 110 °C for 12 h and then 2 M HCl was added. The product was extracted with chloroform. The organic phase was washed successively with 10% sodium bisulfate, 2 M HCl, and water and dried over MgSO_4 . The solvent was removed to afford the product as dark red crystals, which were recrystallized from hot hexane to give the product (2.18 g, 63% yield).

^1H NMR (300 MHz, CDCl_3 , δ , ppm) δ 8.01 (d, 2H), 7.94 (t, 2H), 7.88 (t, 2H), 7.76 (d, 2H). ^{13}C NMR (CDCl_3 , δ , ppm) 134.2, 131.4, 130.4, 129.1, 128.5, 127.1, 126.8, 125.4. Anal. calcd for $\text{C}_{16}\text{H}_8\text{Br}_2$: C, 53.37; H, 2.24; Br, 44.39. Found: C, 53.21; H, 2.20.

General Polymerization Procedure

Three copolymers were synthesized by Stille coupling polymerization.³⁷ The (3,4'-dihexyl-2,2'-bithiophene-5,5'-diyl)bis(trimethylstannane), 4,7-bis(5'-bromo-3'-hexyl-2,2'-bithiophen-5-yl)benzo[c][1,2,5]thiadiazole, and 1,6-dibromopyrene monomers were synthesized according to the methods reported previously. The reaction mixture of tris(dibenzylideneacetone)dipalladium and tri-*o*-tolylphosphine in anhydrous chlorobenzene (15 mL) was stirred at 90 °C for 2 days. Then, an excess amount of 2-bromothiophene and tripropyl(thiophen-2-yl)stannane (the end capper) dissolved in anhydrous chlorobenzene (1 mL) was added, and stirring was continued for 12 h. The reaction mixture was cooled down to room temperature and added slowly to a vigorously stirred mixture of methanol (220 mL) and 1 M HCl (10 mL). The precipitated polymer was collected by filtration and purified by dissolution in chloroform and reprecipitation three times in methanol. The solid was washed for 2 days in a Soxhlet extractor using an acetone/methanol mixture to remove any oligomers and residual catalyst. The final product was obtained after drying under vacuum at 60 °C. The resulting polymers were soluble in common organic solvents.

RESULTS AND DISCUSSION

Synthesis and Characterization of Monomers and Polymers

^1H NMR spectra of the 2,2'-bis(trimethylstannyl)-3,3'-bis(hexyl)-5,5'-bithiophene (M1) and 4,7-bis(5'-bromo-3'-hexyl-

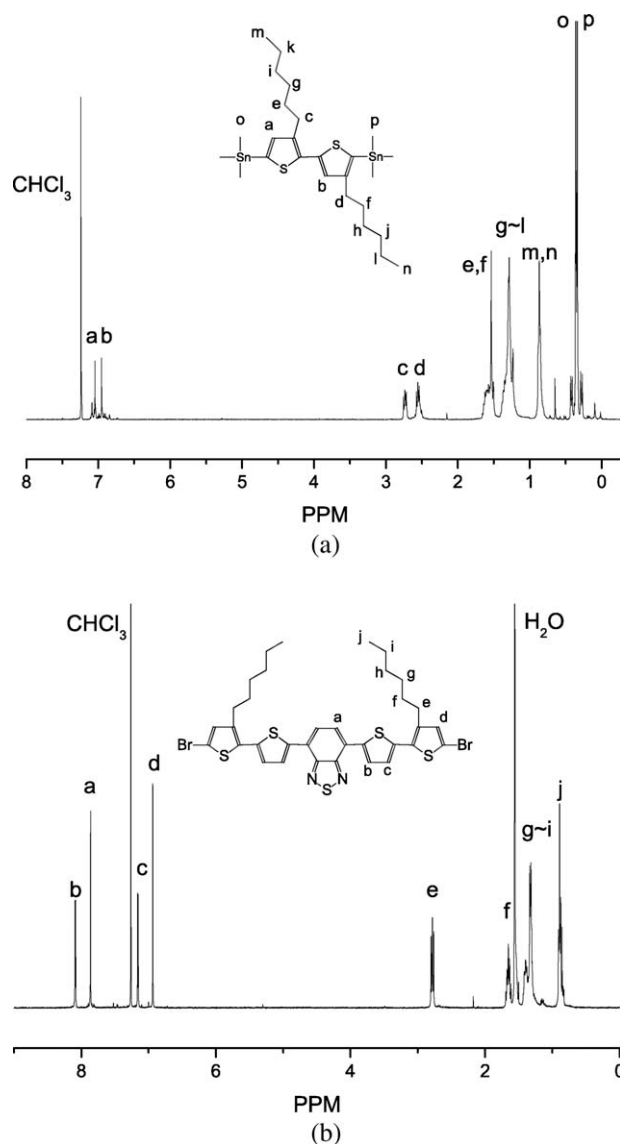


FIGURE 1 ^1H NMR spectra of (a) M1 and (b) M2 units in CDCl_3 solution.

2,2'-bithiophen-5-yl)benzo[c][1,2,5]thiadiazole (M2) monomers are shown in Figure 1(a, b). All the proton peaks are consistent with the corresponding monomer structures. All the polymers were synthesized by polycondensation of bis(arylbromide)s and bis(aryltrimethyltin)s through a Pd(0)-catalyzed Stille coupling reaction. The synthesized polymers showed good solubility in common organic solvents such as chloroform, toluene, and chlorobenzene. The polymer solutions were spin coated onto glass or ITO substrates and formed transparent and homogeneous thin films.

The number-average molecular weights (M_n) of the synthesized polymers were determined by GPC using a polystyrene standard. The M_n values were 5300 g/mol (polydispersity index, PDI = 1.30) for poly(DHBT-*alt*-PYR), 5800 g/mol (PDI = 2.50) for poly(50DHBT-*co*-40PYR-*co*-10BHBTBT), and 6200 g/mol (PDI = 2.00) for poly(50DHBT-*co*-20PYR-*co*-30BHBTBT). The thermal stabilities of the polymers were

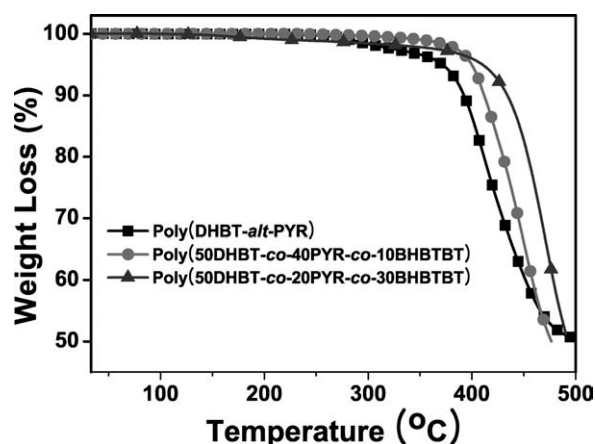


FIGURE 2 TGA thermograms of the polymers with a ramping rate of 10 °C/min.

evaluated by thermogravimetric analysis (TGA) under a N₂ atmosphere. The actual compositions of the resulting *ter*-polymers were determined by elemental analysis using the nitrogen content as the standard. The actual compositions of the copolymers were not the same as the feed ratios, but we found that the differences were not significant. These polymers exhibited good stabilities, showing less than 5% weight loss up to 371–413 °C, as shown in Figure 2. The molecular weights, thermal properties, and actual compositions of the polymers are summarized in Table 1.

Optical Properties

The UV-visible absorption spectra of the polymer solutions in chloroform are shown in Figure 3. Poly(DHBT-*alt*-PYR) showed a strong absorption at 412 nm, corresponding to the π - π^* transition. Interestingly, the absorption bands of the BHBTBT-containing *ter*-polymers moved to longer wavelength regions than that of poly(DHBT-*alt*-PYR). Poly(50DHBT-*co*-40PYR-*co*-10BHBTBT) and poly(50DHBT-*co*-20PYR-*co*-30BHBTBT) exhibited two strong absorption peaks at 403 and 545 nm, respectively. The two peak positions are the same in the two *ter*-polymers, but the relative peak intensity at 545 nm increased with increasing BHBTBT content in the *ter*-polymers. The second absorption band in the *ter*-polymers might be caused by intramolecular charge transfer

between the electron-withdrawing BHBTBT and electron-donating DHBT units.

Figure 4 shows the UV-visible absorption spectra of the polymer thin films. The shapes of the absorption spectra are similar to those of the corresponding polymer solutions, but both the peak positions and onset wavelengths moved to longer wavelength regions because of the enhanced interchain π -interactions. The optical bandgaps (E_g^{opt}) of the polymers were determined from the onset wavelength of the UV-visible spectra of the polymer films. The measured optical bandgap of poly(DHBT-*alt*-PYR) was 2.47 eV, which is very high for photovoltaic applications because the polymer would absorb only a limited portion of the sunlight. The BHBTBT-containing *ter*-polymers, however, showed much lower bandgap energies than poly(DHBT-*alt*-PYR). The optical bandgaps of poly(50DHBT-*co*-40PYR-*co*-10BHBTBT) and poly(50DHBT-*co*-20PYR-*co*-30BHBTBT) were 1.84 and 1.73 eV, respectively. The UV-visible absorption properties and optical bandgap energies of the polymers are summarized in Table 2.

Electrochemical Properties

The electrochemical properties of the polymer films were characterized by CV. The positions of the highest occupied molecular orbitals (HOMOs) of the polymer films were determined by obtaining the oxidation onsets.³⁸ A platinum electrode coated with polymer was used as the working electrode, a platinum wire was used as the counter electrode, and an Ag/AgNO₃ (0.01 M) electrode was used as the reference electrode. The electrochemical properties of the copolymers were investigated in an electrolyte consisting of a solution of 0.1 M TBABF₄ in acetonitrile at room temperature under nitrogen at a scan rate of 50 mV/s. The measurements were calibrated using ferrocene as the standard. The lowest unoccupied molecular orbital (LUMO) energy levels of the polymers were determined by combining the HOMO energy levels obtained from CV and the optical bandgap energies obtained from the edges of absorption.³⁹ The onset oxidation potentials ($E_{\text{ox}}^{\text{onset}}$) of the three polymers were observed in the range of 0.52–0.83 V. The energy level of the Ag/AgNO₃ reference electrode was 4.78 eV below the vacuum level.³⁸ Therefore, the HOMO energy levels were calculated using the equation $\text{HOMO (eV)} = -(E_{\text{ox}}^{\text{onset}} + 4.78)$ (eV), where E_{ox} is the onset oxidation potential versus Ag/Ag⁺. The measured

TABLE 1 Molecular Weights and Thermal Properties of Polymers

| Polymer | Polymer Yield (%) | M_n^a (g/mol) | M_w^a (g/mol) | PDI ^a | T_d^b (°C) | Ratio ^c (DTBT mol %) | |
|---|-------------------|-----------------|-----------------|------------------|--------------|---------------------------------|---------------------------|
| | | | | | | Feed Ratio | Actual Ratio ^d |
| Poly(DHBT- <i>alt</i> -PYR) | 54 | 5,300 | 6,800 | 1.3 | 371 | – | – |
| Poly(50DHBT- <i>co</i> -40PYR- <i>co</i> -10BHBTBT) | 59 | 5,800 | 14,500 | 2.5 | 400 | 10 | 8.2 |
| Poly(50DHBT- <i>co</i> -20PYR- <i>co</i> -30BHBTBT) | 57 | 6,200 | 12,400 | 2.0 | 413 | 30 | 32.1 |

^a M_n , M_w , and PDI of the polymers were determined by GPC using polystyrene standards in CHCl₃.

^b Temperature at 5% weight loss at a heating rate of 10 °C/min under nitrogen.

^c Calculated by elemental analysis through calculation of the amount of nitrogen contained in the copolymers.

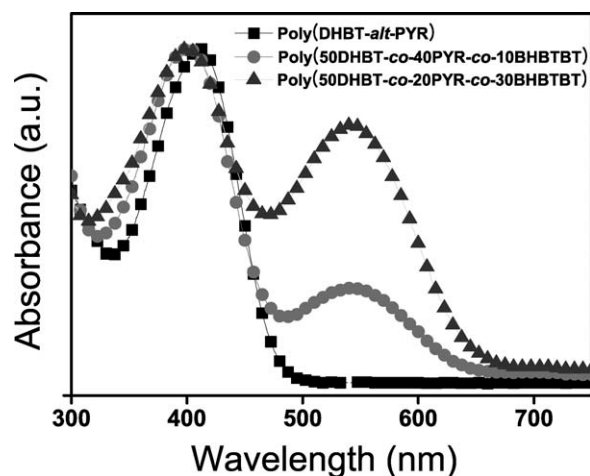


FIGURE 3 UV-visible absorption spectra of the polymers in chloroform solution.

HOMO energy levels of poly(DHBT-*alt*-PYR), poly(50DHBT-*co*-40PYR-*co*-10BHBTBT), and poly(50DHBT-*co*-20PYR-*co*-30BHBTBT) were -5.61 , -5.38 , and -5.30 eV, respectively. Poly(DHBT-*alt*-PYR) showed a relatively low HOMO energy level with the introduction of pyrene units and would have good oxidative stability. The HOMO energy level was increased by reducing the pyrene contents or increasing the BHBTBT content in the polymers. The LUMO energy levels of the polymers were estimated from these HOMO energy levels and optical bandgap energies. The LUMO energy levels, however, moved to lower positions with increasing BHBTBT content in the polymers. The energy diagrams of the polymers, PC₇₁BM, and electrodes are illustrated in Figure 5, and the electrochemical properties and energy-level parameters of the polymers are summarized in Table 2.

TFT Characteristics of the Polymer Thin Films

For the measurement of the field-effect mobility of the charge carriers, OTFTs were fabricated on silicon wafers using a bottom-contact geometry (channel length $L = 12 \mu\text{m}$ width $W = 120 \mu\text{m}$) under nitrogen. The TFT devices of the polymers exhibited typical p-channel transistor characteristics. Figure 6 shows the transfer curves of the devices fabricated using the polymers as the active layer. The field-effect mobility was calculated in the saturation regime using the

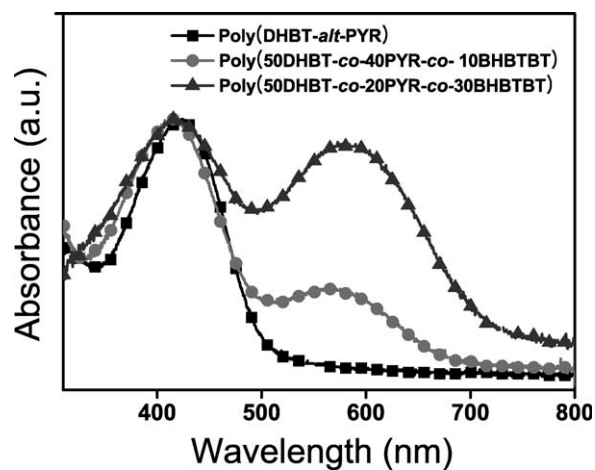


FIGURE 4 UV-visible absorption spectra of the polymer thin films.

following equation: $I_{\text{ds}} = (W/2L)\mu C_i (V_{\text{gs}} - V_{\text{th}})^2$, where I_{ds} is the drain-source current in the saturated region, W and L are the channel width and length, respectively, μ is the field-effect mobility, C_i is the capacitance per unit area of the insulating layer, and V_{gs} and V_{th} are the gate and threshold voltages, respectively.⁴⁰ The measured field-effect mobilities for poly(DHBT-*alt*-PYR), poly(50DHBT-*co*-40PYR-*co*-10BHBTBT), and poly(50DHBT-*co*-20PYR-*co*-30BHBTBT) were determined to be 1.0×10^{-4} , 4.0×10^{-6} , and $1.3 \times 10^{-6} \text{ cm}^2/\text{V s}$, respectively. The alternating copolymer, poly(DHBT-*alt*-PYR), showed the highest mobility among these polymers, suggesting that the regularity of the polymer structure greatly affected the mobility. The mobilities of the *ter*-polymers decreased with decreasing pyrene or increasing BHBTBT contents in the polymers. The characteristics of the TFTs using the polymers as the active layers are summarized in Table 3.

Photovoltaic Devices Properties

Photovoltaic devices were fabricated using the synthesized polymers as p-type electron donors and PC₇₁BM as an n-type acceptor. Photovoltaic devices with ITO/PEDOT:PSS/polymer + PC₇₁BM/LiF/Al configurations were fabricated and characterized. In our preliminary study, we found that the optimum ratio of polymer to PC₇₁BM for these devices was 1:3 by weight, so we prepared active layers with this ratio for the photovoltaic devices.

TABLE 2 Optical and Electrochemical Properties of Polymers

| Polymers | $\lambda_{\text{max, abs}}$ (nm) Solution ^a | λ_{max} (nm) Film ^b | λ_{edge} (nm) Film ^b | Optical $E_{\text{g}}^{\text{opt}}$ (eV) ^c | HOMO (eV) | LUMO (eV) |
|---|--|---|--|--|--------------|--------------|
| Poly(DHBT- <i>alt</i> -PYR) | 412 | 424 | 502 | 2.47 | 5.61 | 3.14 |
| Poly(50DHBT- <i>co</i> -10PYR- <i>co</i> -10BHBTBT) | 403, 545 | 417, 570 | 671 | 1.84 | 5.38 | 3.54 |
| Poly(50DHBT- <i>co</i> -20PYR- <i>co</i> -30BHBTBT) | 403, 545 | 417, 582 | 714 | 1.73 | 5.30 | 3.57 |

^a 1×10^{-5} M in anhydrous chloroform.

^b Polymer film on a quartz plate by spin casting from a solution in chloroform at 1500 rpm for 30 s.

^c Calculated from the absorption band edge of the copolymer films, $E_{\text{g}} = 1240/\lambda_{\text{edge}}$.

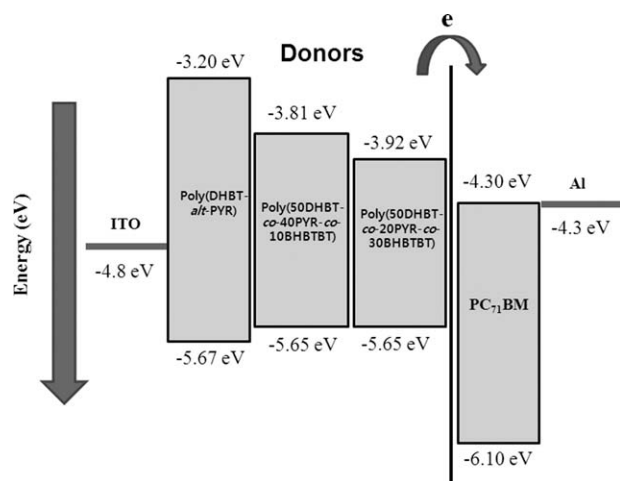


FIGURE 5 Energy band diagram of the polymers, PC₇₁BM, ITO, and Al electrodes.

Figure 7 shows the J - V curves of the OPVs fabricated using the polymers under AM 1.5 illumination (100 mW/cm^2). To achieve the optimum thickness of the active layer, we fabricated photovoltaic devices with different active layer thicknesses from 60 to 100 nm. The fabricated devices showed the highest PCEs when the active layer thickness was 100 nm, as shown in Table 4. All the fabricated devices using the polymers showed relatively high V_{oc} values. The device fabricated using poly(DHBT-*alt*-PYR) showed the highest open-circuit potential ($\approx 0.72 \text{ V}$) of all those fabricated with 100-nm-thick active layers. This is coincident with the measured deep HOMO energy levels of the pyrene-containing polymers. The open-circuit potential of a photovoltaic device is dependent on the energy gap between the HOMO of the donor polymer and the LUMO of the acceptor fullerene. Therefore, donor polymers that have deep HOMO energy levels are desirable for the fabrication of photovoltaic devices with high open-circuit voltages.

Incidentally, the short-circuit currents of the devices are increased upon increasing the BHBTBT contents in the polymers. As shown in the UV-visible absorption spectra in Figure 3, as the number of BHBTBT units in the copolymer was increased in the polymers, the absorption in regions of longer wavelength increased. This increasing light absorption increased the short-circuit currents of the photovoltaic devices. The device using poly(50DHBT-*co*-20PYR-*co*-30BHBTBT) showed the highest J_{sc} among the fabricated devices. This result, however, contradicts the mobility data of the polymers in the previous section, because poly(50DHBT-*co*-

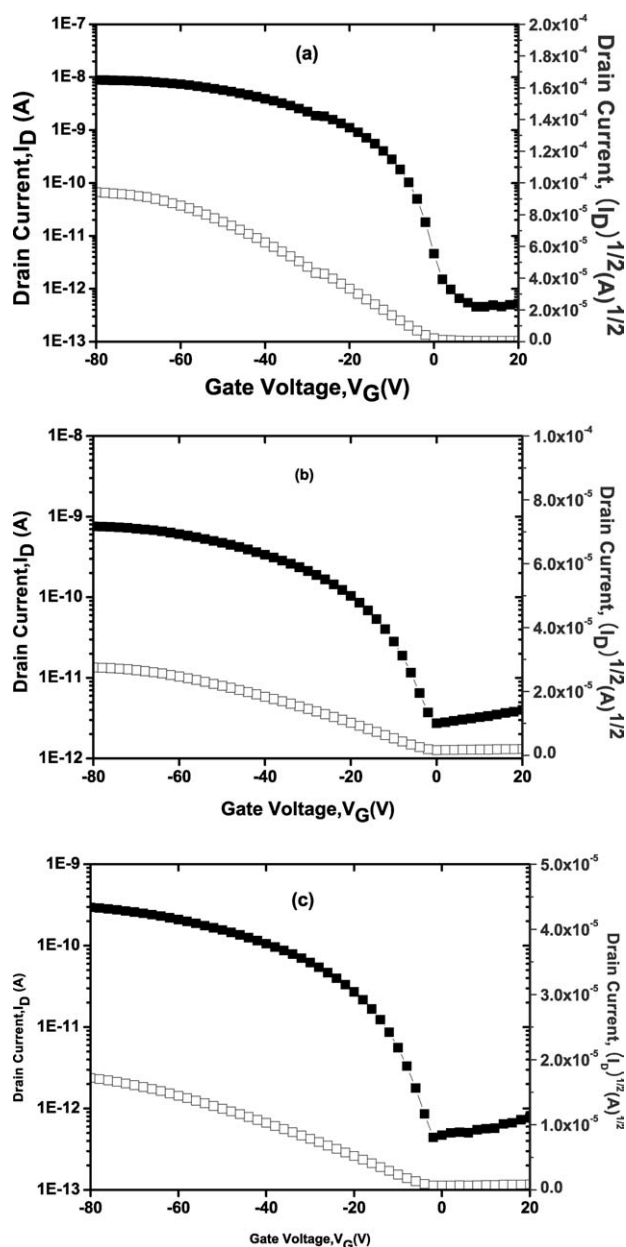


FIGURE 6 Transfer characteristics of OTFTs fabricated using the polymers as the active layers at a constant source-drain voltage of -80 V . (a) Poly(DHBT-*alt*-PYR), (b) poly(50DHBT-*co*-40PYR-*co*-10BHBTBT), and (c) poly(50DHBT-*co*-20PYR-*co*-30BHBTBT).

20PYR-*co*-30BHBTBT) showed the lowest mobility of the three polymers. Both the mobility and light absorption may affect the short-circuit currents of PSCs, but in our results,

TABLE 3 Summary of the Characteristics of OTFTs Fabricated Using the Polymers as the Active Layers

| Polymer | Poly(DHBT- <i>alt</i> -PYR) | Poly(50DHBT- <i>co</i> -40PYR- <i>co</i> -10BHBTBT) | Poly(50DHBT- <i>co</i> -20PYR- <i>co</i> -30BHBTBT) |
|---------------------------------------|-----------------------------|---|---|
| Mobility ($\text{cm}^2/\text{V s}$) | 1.0×10^{-4} | 4.0×10^{-6} | 1.3×10^{-6} |
| I_{on}/I_{off} | 10^4 | 10^2 | 10^3 |

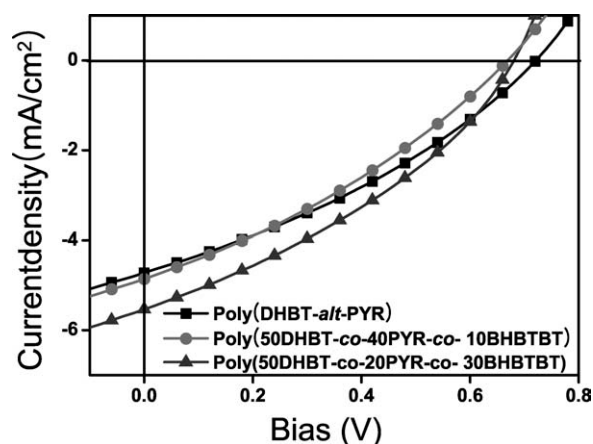


FIGURE 7 J - V curves for the polymer:PC₇₁BM (1:3 wt %) solar cell devices.

the light absorption (not the polymer mobility) would be the major factor affecting the short-circuit currents of the devices.

The short-circuit currents of the devices with 100-nm active layers fabricated using poly(DHBT-*alt*-PYR), poly(50DHBT-*co*-40PYR-*co*-10BHBTBT), and poly(50DHBT-*co*-20PYR-*co*-30BHBTBT) were 4.72, 4.86, and 5.54 mA/cm², respectively. Interestingly, the photovoltaic device using poly(DHBT-*alt*-PYR) showed a PCE of 1.13%, even though it had a very wide bandgap energy (\approx 2.47 eV). This may be because of the relatively high hole mobility of poly(DHBT-*alt*-PYR) and the high V_{oc} due to the deep HOMO energy level of the polymer. To our knowledge, this would be one of the highest PCEs among the OPVs fabricated using semiconducting polymers with similar bandgap energies to poly(DHBT-*alt*-PYR).

The highest PCE among our fabricated devices was obtained using the poly(50DHBT-*co*-20PYR-*co*-30BHBTBT)/PC₇₁BM active layer with a thickness of 100 nm. The measured PCE was 1.31%, with J_{sc} of 5.54 mA/cm², V_{oc} of 0.68 V, and a FF

of 0.35 under AM 1.5 G irradiation (100 mW/cm²). The corresponding V_{oc} , J_{sc} , FF, and PCE values of the devices made under different device fabrication conditions are summarized in Table 4. The accuracy of the photovoltaic measurements can be confirmed by the external quantum efficiency (EQE) of the devices.

Figure 8 shows the EQE curves of the PSCs fabricated under the same optimized conditions as those used for the J - V measurements. Obviously, the EQE values of poly(50DHBT-*co*-20PYR-*co*-30BHBTBT) are higher than those of poly(DHBT-*alt*-PYR) and poly(50DHBT-*co*-40PYR-*co*-10BHBTBT), in agreement with the higher J_{sc} values of the devices derived from poly(50DHBT-*co*-20PYR-*co*-30BHBTBT). To evaluate the accuracy of the photovoltaic results, we calculated the J_{sc} values by integrating the EQE data with the AM 1.5 G reference spectrum. The J_{sc} values obtained by integration and the J - V measurements are rather close. The onset wavelength of the photon-to-current conversion was 750 nm for all the devices.

The surface morphologies of the polymers and PC₇₁BM blend films were observed by tapping-mode atomic force microscopy (AFM). The blend films showed almost equivalently measured smooth surfaces [according to their root-mean-square (RMS) roughness] with small degrees of phase separation. As shown in Figure 9, the RMS roughness of the active layers was 2.00 nm for poly(DHBT-*alt*-PYR), 0.98 nm for poly(50DHBT-*co*-40PYR-*co*-10BHBTBT), and 1.81 nm for poly(50DHBT-*co*-20PYR-*co*-30BHBTBT). Compared with the poly(DHBT-*alt*-PYR):PC₇₁BM blend film, the poly(50DHBT-*co*-40PYR-*co*-10BHBTBT):PC₇₁BM blend film showed a flatter surface with an RMS of 0.98 nm [Fig. 9(b)], and no obvious phase separation was observed. As poly(50DHBT-*co*-40PYR-*co*-10BHBTBT) and PC₇₁BM molecules have good miscibility, an increased interfacial area was expected, and the J_{sc} value of the poly(50DHBT-*co*-40PYR-*co*-10BHBTBT):PC₇₁BM-based device increases to 4.86 mA/cm², which was nearly 0.15 mA/cm² higher than that of the poly(DHBT-*alt*-PYR):PC₇₁BM-based device. In the case of the poly(50DHBT-*co*-20PYR-*co*-

TABLE 4 Summary of the Properties of Photovoltaic Devices Fabricated Using Composites of the Polymers and PC₇₁BM (1:3 Ratio)

| Polymer | Thickness (nm) | V_{oc}^a (V) | J_{sc}^a (mA/cm ²) | FF ^a | PCE ^a (%) |
|---|----------------|----------------|----------------------------------|-----------------|----------------------|
| Poly(DHBT- <i>alt</i> -PYR) | 60 | 0.76 | 2.35 | 0.29 | 0.52 |
| | 80 | 0.74 | 4.33 | 0.32 | 1.03 |
| | 100 | 0.72 | 4.72 | 0.33 | 1.13 |
| Poly(50DHBT- <i>co</i> -40PYR- <i>co</i> -10BHBTBT) | 60 | 0.67 | 2.47 | 0.28 | 0.47 |
| | 80 | 0.70 | 4.62 | 0.30 | 0.98 |
| | 100 | 0.67 | 4.86 | 0.32 | 1.05 |
| Poly(50DHBT- <i>co</i> -20PYR- <i>co</i> -30BHBTBT) | 60 | 0.67 | 2.65 | 0.28 | 0.50 |
| | 80 | 0.69 | 5.44 | 0.33 | 1.23 |
| | 100 | 0.68 | 5.54 | 0.35 | 1.31 |

^a Photovoltaic properties of copolymer/PC₇₁BM-based devices spin coated from a 1,2-dichlorobenzene solution of polymer.

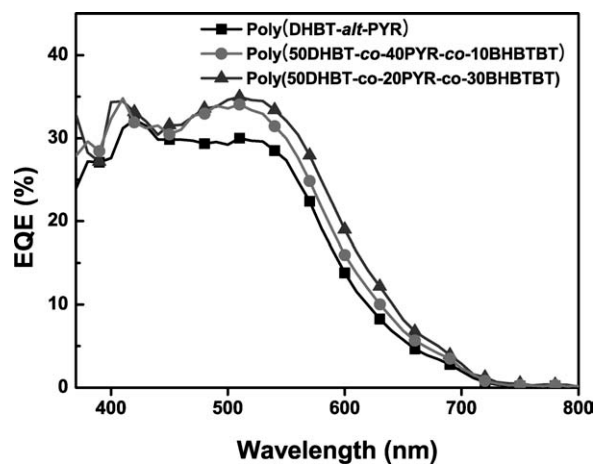


FIGURE 8 IPCE spectra of the polymers:PC₇₁BM (1:3 wt %) solar cell devices.

30BHBTBT) blend film [Fig. 9(c)], uniform phase separation was observed. However, the film from poly(50DHBT-co-20PYR-co-30BHBTBT) and PC₇₁BM showed clear domains with a higher RMS value of 1.81 nm, which is helpful for charge separation, and thus improved the FF of the device. Thus, the large domain size for poly(50DHBT-co-20PYR-co-30BHBTBT) suggests that even better device performance can be expected through further device engineering, for example, by thermal annealing, solvent annealing, and the use of additives to promote proper phase separation.

CONCLUSIONS

A series of π -conjugated polymers composed of head-to-tail-structured bithiophene, pyrene, and bis(bithiophene) conjugated benzothiadiazole derivatives were synthesized by the polycondensation of bis(arylbromide)s and bis(aryltrimethyltin)s through a Pd(0)-catalyzed Stille coupling reaction. Poly(DHBT-alt-PYR) showed a large bandgap energy (2.47 eV) even though it has a relatively high hole mobility. By introducing BHBTBT units into the polymer, we could reduce the

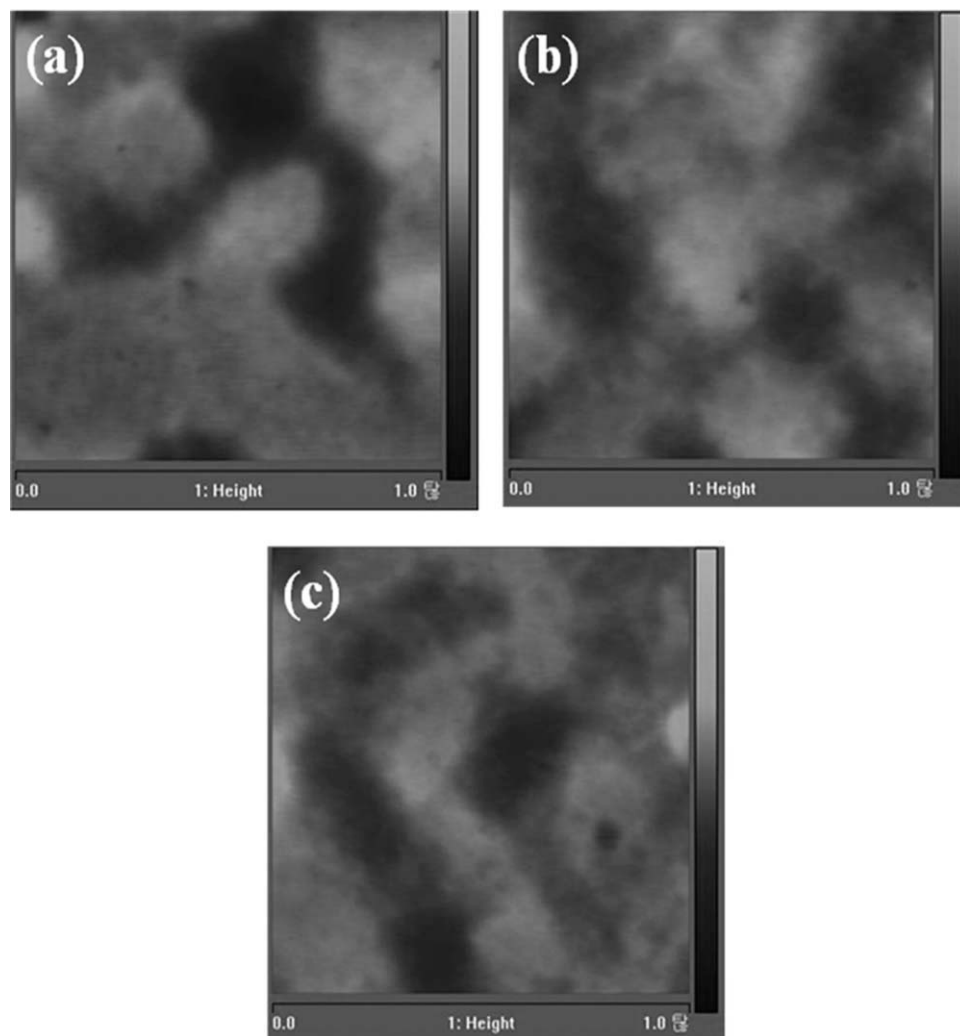


FIGURE 9 Tapping-mode AFM height images of thin films cast from (a) poly(DHBT-alt-PYR):PC₇₁BM (1:3), (b) poly(50DHBT-co-10PYR-co-10BHBTBT):PC₇₁BM (1:3), and (c) poly(50DHBT-co-20PYR-co-30BHBTBT):PC₇₁BM (1:3).

bandgap energies of the resulting poly(DHBT-co-PYR-co-BHBTBT)s. The bandgap energies of poly(50DHBT-co-40PYR-co-10BHBTBT) and poly(50DHBT-co-20PYR-co-30BHBTBT) were 1.84 and 1.73 eV, respectively. All the synthesized polymers showed low HOMO energy levels and high open-circuit voltages in the photovoltaic devices fabricated using them. The device fabricated using poly(50DHBT-co-20PYR-co-30BHBTBT) exhibited the highest PCE of 1.31% under AM 1.5 G illumination conditions (100 mW/cm²).

ACKNOWLEDGMENTS

This research was financially supported by the Ministry of Knowledge Economy (MKE) under the New & Renewable Energy Program through a KETEP grant (No. 20103020010050 and No. 2011T100200034) and by a National Science Foundation (NRF) grant funded by the Korean Government (MEST) (No. 2011-0011122) through GCRC-SOP (Grant No. 2011-0030668).

REFERENCES AND NOTES

- McCullough, R. D.; Lowe, R. D. *J. Chem. Soc. Chem. Commun.* **1992**, 1, 70–72.
- Chen, T.-A.; Rieke, R. D. *J. Am. Chem. Soc.* **1992**, 114, 10087–10088.
- Chen, T.-A.; Wu, X.; Rieke, R. D. *J. Am. Chem. Soc.* **1995**, 117, 233–244.
- Cho, S.; Lee, K.; Yuen, J.; Wang, G.; Moses, D.; Heeger, A. J.; Surin, M.; Lazzaroni, R. J. *J. Appl. Phys.* **2006**, 100, 114503–1–114503-6.
- Ong, B. S.; Wu, L. Y.; Liu, P.; Gardner, S. J. *Am. Chem. Soc.* **2004**, 126, 3378–3379.
- McCulloch, I.; Heeney, M.; Bailey, C.; Genevicius, K.; Macdonald, I.; Shkunov, M.; Sparrowe, D.; Tierney, S.; Wagner, R.; Zhang, W.; Chabinyc, M. L.; Kline, R. J.; McGehee, M. D.; Toney, M. F. *Nat. Mater.* **2006**, 5, 328–333.
- Shaheen, S. E.; Vangeneugden, D.; Kiebooms, R.; Vanderzande, D.; Fromherz, T.; Padinger, F.; Brabec, P. C. J.; Sariciftci, N. S. *Synth. Met.* **2001**, 121, 1583–1584.
- Vangeneugden, D. L.; Vanderzande, D. J. M.; Salbeck, J.; Van Hal, P. A.; Janssen, R. A. J.; Hummelen, J. C.; Brabec, C. J.; Shaheen, S. E.; Sariciftci, N. S. *J. Phys. Chem. B* **2001**, 105, 11106–11113.
- Hou, J.; Park, M. H.; Zhang, S.; Yao, Y.; Chen, L. M.; Li, J. H.; Yang, Y. *Macromolecules* **2008**, 41, 6012–6018.
- Bundgaard, E.; Krebs, F. C. *Macromolecules* **2006**, 39, 2823–2831.
- Bundgaard, E.; Krebs, F. C. *Sol. Energy Mater. Sol. Cells* **2007**, 91, 1019–1025.
- Li, J.-C.; Beak, M.-J.; Kwon, J.-T.; Lee, E.-W.; Lee, S.-H.; Lee, Y.-S. *Macromol. Res.* **2010**, 18, 1237–1240.
- Jo, P. S.; Park, Y. J.; Kang, S. J.; Kim, T. H.; Park, C. *Macromol. Res.* **2010**, 18, 777–786.
- Krebs, F. C.; Gevorgyan, S. A.; Alstrup, J. J. *Mater. Chem.* **2009**, 19, 5442–5451.
- Krebs, F. C.; Fyenbo, J.; Tanenbaum, D. M.; Gevorgyan, S. A.; Andriessen, R.; Remoortere, B.; Galagan, Y.; Jørgensen, M. *Energy Environ. Sci.* **2011**, 4, 4116–4123.
- Jørgensen, M.; Norrman, K.; Gevorgyan, S. A.; Tromholt, T.; Andreasen, B.; Krebs, F. C. *Adv. Mater.* **2012**, 24, 580–612.
- Dimitrakopoulos, C. D.; Purushothaman, S.; Kymissis, J.; Callegari, A.; Shaw, J. M. *Science* **1999**, 283, 822–824.
- Sirringhaus, H.; Tessler, N.; Friend, R. H. *Science* **1998**, 281, 1741–1744.
- Dennler, G.; Scharber, M.; Brabec, C. J. *Adv. Mater.* **2009**, 21, 1323–1338.
- Kim, J. Y.; Kim, S. H.; Lee, H.-H.; Lee, K.; Ma, W.; Gong, X.; Heeger, A. J. *Adv. Mater.* **2006**, 18, 572–576.
- Ma, W. L.; Yang, C. Y.; Gong, X.; Lee, K.; Heeger, A. J. *Adv. Funct. Mater.* **2005**, 15, 1617–1622.
- Chen, H.-Y.; Hou, J.; Zhang, S.; Liang, Y.; Yang, G.; Yang, Y.; Yu, L.; Wu, L.; Li, G. *Nat. Photon.* **2009**, 3, 649–653.
- Hou, J. H.; Huo, L. J.; He, C.; Yang, C. H.; Li, Y. F. *Macromolecules* **2006**, 39, 594–603.
- Zhang, Z.-G.; Liu, Y.-L.; Yang, Y.; Hou, K.; Peng, B.; Zhao, G. J.; Zhang, M. J.; Guo, X.; Kang, E.-T.; Li, Y. F. *Macromolecules* **2010**, 43, 9376–9383.
- Huo, L. J.; Hou, J. H.; Chen, H.-Y.; Zhang, S. Q.; Jiang, Y.; Chen, T. L.; Yang, Y. *Macromolecules* **2009**, 42, 6564–6571.
- Huo, L. J.; Tan, Z. A.; Wang, X.; Zhou, Y.; Han, M. F.; Li, Y. F. *J. Polym. Sci. Part A: Polym. Chem.* **2008**, 46, 4038–4049.
- Scharber, M. C.; Mühlbacher, D.; Koppe, M.; Denk, P.; Waldauf, C.; Heeger, A. J.; Brabec, C. J. *Adv. Mater.* **2006**, 18, 789–794.
- Wang, E. G.; Wang, L.; Lan, L. F.; Luo, C.; Zhuang, W. L.; Peng, J. B.; Cao, Y. *Appl. Phys. Lett.* **2008**, 92, 033307–1–033307-3.
- Svensson, M.; Zhang, F. L.; Veenstra, S. C.; Verhees, W. J. H.; Hummelen, J. C.; Kroon, J. M.; Inganäs, O.; Andersson, M. R. *Adv. Mater.* **2003**, 15, 988–991.
- Blouin, N.; Michaud, A.; Leclerc, M. *Adv. Mater.* **2007**, 19, 2295–2300.
- Liang, Y.; Xu, Z.; Xia, J.; Tsai, S.-T.; Wu, Y.; Li, G.; Ray, C.; Yu, L. *Adv. Mater.* **2010**, 22, E135–E138.
- Price, S. C.; Stuart, A. C.; Yang, L.; Zhou, H.; You, W. J. *Am. Chem. Soc.* **2011**, 133, 4625–4631.
- Ashizawa, M.; Yamada, K.; Fukaya, A.; Kato, R.; Hara, K.; Takeya, J. *Chem. Mater.* **2008**, 15, 4883–4890.
- Coleman, A.; Pryce, M. T. *Inorg. Chem.* **2008**, 47, 10980–10990.
- Zhang, H.; Wang, Y.; Shao, K.; Liu, Y.; Chen, S.; Qiu, W.; Sun, X.; Qi, T.; Ma, Y.; Yu, G.; Su, Z.; Zhu, D. *Chem. Commun.* **2006**, 46, 755–757.
- Sahu, D.; Padhy, H.; Patra, D.; Kekuda, D.; Chu, C.-W.; Chiang, I.-H.; Lin, H.-C. *Polymer* **2010**, 51, 6182–6192.
- Kim, J.; Park, S. H.; Cho, S.; Jin, Y.; Kim, J.; Kim, I.; Lee, J. S.; Kim, J. H.; Woo, H. Y.; Lee, K.; Suh, H. *Polymer* **2010**, 51, 390–396.
- Chen, G. Y.; Cheng, Y. H.; Chou, Y. J.; Su, M. S.; Chen, C. M.; Wei, K. H. *Chem. Commun.* **2011**, 47, 5064–5066.
- Li, Y. F.; Cao, Y.; Gao, J.; Wang, D. L.; Yu, G.; Heeger, A. J. *Synth. Met.* **1999**, 99, 243–248.
- Shaw, J. M.; Seidler, P. F. *IBM J. Res. Dev.* **2001**, 45, 3–9.